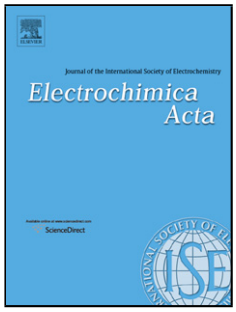

Title: Voltammetric determination of epinephrine and xanthine based on sodium dodecyl sulphate assisted tungsten trioxide nanoparticles

Authors: A.C. Anithaa, K. Asokan, C. Sekar

PII: S0013-4686(17)30570-4
DOI: http://dx.doi.org/doi:10.1016/j.electacta.2017.03.098
Reference: EA 29132

To appear in: *Electrochimica Acta*

Received date: 24-11-2016
Revised date: 12-3-2017
Accepted date: 14-3-2017

Please cite this article as: A.C.Anithaa, K.Asokan, C.Sekar, Voltammetric determination of epinephrine and xanthine based on sodium dodecyl sulphate assisted tungsten trioxide nanoparticles, Electrochimica Actahttp://dx.doi.org/10.1016/j.electacta.2017.03.098

<AT>Voltammetricdetermination ofepinephrine and xanthine based on sodium dodecyl sulphate assisted tungsten trioxide nanoparticles

<AU>A.C. Anithaa[a], K. Asokan[b], C. Sekar[a,*] ##Email##Sekar2025@gmail.com##/Email##
<AU>

<AFF>[a]Dept. of Bioelectronics and Biosensors, Alagappa University, Karaikudi 630003, TN, India
<AFF>[b]Materials Science Division, Inter-University Accelerator Centre, New Delhi 110067, India

<PA>*Tel.: +91 9442563637*.

<ABS-Head><ABS-HEAD>Graphical abstract
<ABS-P>► The gamma ray irradiated (50 kGy) sodium dodecyl sulphate (SDS) assisted tungsten trioxide (WO_3) nanoparticles with columnar polyhedron morphology acts as an excellent electrocatalyst which remarkably manifested the simultaneous determination of epinephrine and xanthine.
<ABS-HEAD>Highlights► A novel electrochemical sensor has been developed for the simultaneous determination of epinephrine and xanthine based on gamma irradiated SDS-WO_3 NPs for the first time. ► The fabricated sensor exhibits wide linear range (0.009-1000 μM), low detection limit (1.8 nM for EP and 2.2 nM for XA), good stability and reproducibility. ► The proposed method was successfully applied to the analysis of human serum samples with satisfactory results.
<ABS-HEAD>ABSTRACT
<ABS-P>This work reports the voltammetric determination of epinephrine (EP) and xanthine (XA) using gamma irradiatedtungsten trioxide (WO_3) nanoparticles. WO_3 NPs synthesized by anionic surfactant sodium dodecyl sulphate (SDS) assisted template method was subjected to gamma rays under different doses (0-150 kGy). The experimental results revealed that the 50 kGy irradiation on SDS-WO_3 NPs led to significant changes in crystallite size and morphology which enriched its electrocatalytic activity greatly. The electrochemical behaviors of EP and XA at 50 kGy SDS-WO_3 modified glassy carbon electrodes (GCE) were studied by cyclic voltammetry and differential pulse voltammetry. The outcomes confirmed that the proposed electrode demonstrateexcellent electrocatalytic activity towardsthe oxidation of EP and XA in phosphate buffer solution (PBS, pH 7.0). The fabricated electrode possess lowest detection limit of 1.8 nM and 2.2 nM for EP and XA respectively with the very wide dynamic linear range of 9 nM to 1 mM. Finally, the modified sensor was successfully implemented to detect EP and XA in the human serum samples with excellent selectivity, good stability and reproducibility.
<KWD>Keywords: Tungsten trioxide; SDS; Gamma irradiation;Epinephrine; Xanthine;

Electrochemical sensor.

<H1>1. Introduction

Epinephrine (4-[(1R)-1-Hydroxy-2-(methylamino) ethyl]-1,2-benzenediol, EP) also known as adrenaline, is an essentialendocrine hormone released from the adrenal glandwhich play vital role on glycogen metabolism and nervous system [1,2]. In adults, the concentration of EP are

normally less than 10 ng/L, but may increase by 10-fold during exercise andby 50-fold in blood and urine during stressdue to activation of the sympatho-adrenal system [3,4]. The concentration of EP affects glycogenolysis in liver and skeletal muscle, lipolysis in adipose tissue, plasma lactate andrate of heart contraction [5].Low levels of EPhave been found in patients with Parkinson'sdisease. Due to such physiological effects, this vasopressor drug has been banned to practice in games by world anti-doping agency and has medicalapplications for patients with diseases such as cardiac arrest, asthma and sepsis in emergency cases [6].

Xanthine (3,7-dihydro-purine-2,6-dione, XA), an intermediate metabolite of purine nucleotide and deoxynucleotide metabolism in humans,is formed after adenosine triphosphate (ATP)decomposition [7,8].Abnormal concentration ofXA levelproduced from the degradation of adenosine and inosine nucleosides causesLesch-Nyhan syndrome[9]. On the other hand,decreased XA activity leads to xanthinuria, which is a rare genetic disorder that causes health problems such as renal failure, kidneystone formation and urinary tract disease [10,11].The physiological conversion of XA to uric acid (UA) by xanthine oxidase is of great interest in the medical field, as this reaction is related to the formation of superoxide radical anion, one of the reactive oxygen species involved in the cancer aging, neurodegenerative diseases such as Parkinson's diseaseand inflammation [12].Normally in our body fluids, biomolecules such as ascorbic acid (AA), UA, EP and XA are usually coexisted and oxidized at a potential close to each other at naked electrodes and interfere with each other for the determination of any one of the analytes.Hence, there is a rising need for persistent development of a novel, simple and sensitive analytical methodfordetermining EP and XA for both research and clinical applications.Here, we report the construction of an electrochemical sensor using gamma irradiated SDS assisted WO_3NPs for the first time.

Nanostructured transition metal oxides (TMO) exhibit the development of new sensors due to their chemical and physical properties leading to numerous potentialapplications. Tungsten trioxide (WO_3), an indirect n type semiconductor, exhibits fascinating electronic, structural and mechanical properties with a wide range of applications in the area of gas sensors, photocatalysis andcatalysis in electrochemical process and smart windows [13]. In order to improve the physic-chemical properties of $WO_{3-\delta}$ nanoparticles, different strategies such as microwave route [14], surfactant mediated method [15,16] and precipitation method [17] have been adopted.Surfactant assisted template synthesis has received considerable attention because the physical andchemical properties of nanostructure materials are strongly related to morphology controllability,simplicity, speed and ease of operation [18].Huo et al. have developed surfactant templating strategies for the synthesis process in order to enhance the surface activity of the materials [19]. Particularly anionic surfactant(Sodium dodecyl sulphate, SDS) employed tosynthesize controlled production of WO_3 NPs with different surface morphology dueto their flexible processing chemistry with hydrophobic carbontail and a hydrophilic head made up of sulfate group, inexpensive organic stabilizer, melting point (206° C),easily soluble in water andbiocompatibility [20].The electrostatic interactions between surfactant molecules andcharged orpolarized metal-oxy precursors generate metastable modified metal oxides [21].Furthermore to enhance the properties of WO_3 NPs, irradiation of WO_3 with higher energeticionizing radiation such as gamma irradiation produces significant changes in the microstructural and morphological properties of WO_3NPs and creates a wide variety of defects, which in turn modify theirelectrochemical sensing properties [22]. Therefore, the investigation of damages or defects and their effects on the sensing behavior of surfactant template on WO_3 NPs plays a major role.

Earlier, we have successfully synthesized WO_3 NPs by gamma irradiation method without the surfactant template and fabricated electrochemical sensor for the detection of serotonin [23]. **In the current work, we investigate about the impact of gamma ray irradiation (0-150 kGy) on the morphological, optical and electrochemical behaviour of SDS assisted WO_3NPs for the first time. Cyclic voltammetry studies of 50 kGy GI SDS-WO_3/GCE on EP and XA oxidation exhibited a remarkable catalytic performance in 0.1 M phosphate buffer solution (pH 7.0). The developed sensor exhibited wide linear dynamic concentration range, lowest detection limit,long term stability and good reproducibility in response to EP and XA.**

<H1>2. Experimental

<H2>2.1 Reagents

Epinephrine and Xanthine were purchased from Alfa Aesar, Mumbai. Tungstic acid, sodium dodecyl sulphate, and 0.1 N sodium hydroxide solutions were purchased from Fischer Scientific, Mumbai.

<H2>2.2. Apparatus

Powder X-ray diffraction (XRD) patterns were documented using a Bruker AXS D8, Germany advanced diffractometer in the range of 20-80º. Energy bandgap values were calculated using UV-Visible spectrophotometer (Thermoscientific-Evolution 201, USA). FESEM images and EDAX spectra were performed using FEG QUANTA 250, Netherland.Electrochemical experiments were executed using a CHI 609D electrochemical workstation (CHI, USA) in conventionalthree-electrode cell system. Glassy carbon electrode (GCE) was used as the working electrode, with a platinum wire as a counter electrode and Ag/AgCl as a reference electrode. The differential pulse voltammetry (DPV) measurements were accomplished in 0.1 M PBS (pH 7.0) in the potential region from 0 to 1.0 V with amplitude of 50 mV and pulse width of 0.06 s.

<H2>2.3. Synthesis of SDS assisted WO_3 NPs

The precursor solution was prepared by dissolving 1 M of tungstic acid (H_2WO_4) in 10 mL sodium hydroxide (NaOH) solution. This resulted in hydrated sodium tungstate solution due to proton exchange protocol process [23]. Subsequently, 50 wt% of SDS was added to the precursor solution to act as ananionic surfactant. In order to enrich the protonation process, HCl was introduced into the solution to attain the pH value of 1. The final solution was exposed to microwave (2.45 GHz) under the optimum power of 180 W for 15 min and dried at 100°C in air.The above process was repeated without adding SDS under identical conditions. The presence of SDS in the colloid limits the particle nucleation and growth which controls the size and morphology of WO_3 NPs. The resulted products were irradiated using Gamma Chamber 1200 (1.25 MeV ^{60}Co source) at IUAC, New Delhi. WO_3 NPs were exposed to different doses (50, 100 and 150 kGy) at room temperature and the activity at the time of exposure was 5.499 kGy/hr.

<H2>2.4 Fabrication of SDS-WO_3 NPs modified GCE

GCEs were polished to a mirror-like surface with 0.30 and 0.50 μm alumina powder sequentially and sonicated in ethanol and water respectively for 5 minutes. The pristine WO_3NPs and gamma irradiated SDS-WO_3 NPs suspension were prepared by dispersing it (5 mg) in 1.0 mL of

deionised water. Then a known amount of WO_3 suspension (10 μL) was dropcasted onto the GCE surface and left to air-dry at room temperature overnight to obtain WO_3 modified GCE.

<H1>3. Results and Discussion

<H2>3.1 Structural and optical characterization of gamma irradiated SDS-WO_3 NPs

Powder XRD patterns of the as prepared and irradiated SDS-WO_3 NPs at various dosages are shown in**Fig. 1A**. All the observed peaks of both non-irradiated and gamma irradiated SDS-WO_3 NPs correspond to the monoclinic structure according to JCPDS data (720677). It can be noticed that there is a significant increase in the diffraction peak intensity for the irradiated samples and that the intensities increase with the increase in the gamma ray dosage levels. This could be attributed to the localized heating occurrence during the exposure of gamma rays. The WO_3 NPs retained its phase even after intensive gamma irradiation, suggesting that the organic additive(SDS) acts as the sizeand morphology controller without affecting the crystalline structure of the WO_3 NPs [24].

UV-Visible spectroscopy studies were performed on all the samples over the range of 200-800 nm, as shown in **Fig. 1B**. The broad absorption peak around 350 to 500 nm was observed in all the samples. The gamma irradiated (50 kGy) NPs display hypochromic shift in the absorbance spectra when compared to the unirradiated and other irradiated SDS-WO_3 NPs.The band gap energy (Eg) of non-irradiated SDS-WO_3 NPs was found to be 3.13 eV which is the intrinsic value for monoclinic WO_3[14]. There is a slight decrease in Eg value for 50 kGy gamma irradiated SDS-WO_3 when compared to that of pristine SDS WO_3 which could be attributed to the induced structural disorder and formation of charge trapping of the radiolytic electrons or holes. Contrary to this, the subsequent increase in doses (100 and 150 kGy) enhances the band gap energy due to the aggregation of WO_3 crystallites and localized heating caused by the irradiation.

<Preferred positionof Fig. 1>

<H2>3.2 Morphological characterization of gamma irradiated SDS-WO_3 NPs

Surface morphology of the pristine and gamma irradiated SDS-WO_3 NPs were examined using FESEM (**Fig. 2**). The pristine sample shows cauliflower like morphology with agglomerated near spherical shaped nanoparticles. After gamma irradiation, the agglomerated particles tend to fragmentand form columnar polyhedron like morphology. In particular, the edges of the polyhedron were sharp and the facets were found to be dented for 50 kGyirradiation as shown in Fig. 2(b).This unique morphology is expected to act as trapping centresfor the biomolecules. At higher dosages (100 and 150 kGy), the edges of the polyhedrons were destroyed leading to the spherical shape (Fig. 2 (c &d)).The high-magnification FESEM imagesshown in the inset of**Fig. 2** revealed that the gamma irradiation on SDS-WO_3 NPs plays a dynamic role on the shape and size depending on the dosage level.Energy dispersive X-ray spectroscopy (EDX) analysis further confirmed the oxygen loss during gamma irradiation with increasing dosages(see Fig. S1).

< Preferred position of Fig. 2>

<H2>3.3 Electrochemical behaviors of EPand XA using GI SDS-WO_3 modified electrode

Cyclic voltammetry (CV) studies were carried out to understandthe electrochemical behavior of EP and XA at different modified electrodes.**Fig. 3A** shows the CVs obtained for 10 µM EP at bare and modified GCEs in 0.1 M PBS (pH 7) at scan rate of 50 mVs^{-1}.At bare GCE, a broad oxidation wave was observed for EP at about 0.33Vwith poorresponse current signifying slow electron transfer kinetics at GCE. On the other hand, the peak potential was slightly reduced to 0.28 V without noticeable improvement in the peak current at pristine WO_3/GCE. However, under the identical conditions, large improvement in the redox peak current (nearly 3-fold)and significant lowering of peak potential to 0.22 V were observed for the electrochemical oxidation of EP at 50 kGy GI SDS-WO_3 modified GCE surface, when compared to bare, pristine SDS-WO_3 and other gamma irradiated SDS-WO_3 modified GCEs. The observed improvement in the electrocatalytic activity of the gamma irradiated SDS-WO_3 NPs for a particular dosage of 50 kGy could be attributed to large electroactive surface area and enhanced electron transfer process. The electrochemical reaction mechanism of EP at 50 kGy GI SDS-WO_3/GCE for the first 3 cycles is shown in the inset of Fig.3A. In the first cycle, the prominent oxidation and reduction peaks were observed at 0.22 and -0.20 V (curve c1), respectively corresponding to the oxidation of EP to epinephrinequinone(EPQ) by the deprotonation process and subsequently, EPQ cyclises to epinephrinechrome via 1,4-Micheal addition reaction at +0.20 V which is less favorable [25].The prominent reduction peak at -0.20 V corresponds to the reduction of epinephrinechrome to leucoepinephrinechrome. In the subsequent 2 cycles, a new oxidation wave was appeared at -0.15 V attributed to the reversible oxidation ofleucoepinephrinechrome to epinephrinechrome. The small oxidation peak at 0.12 V corresponds to the conversion of leucoepinephrinechrome to5,6-dihydroxyl-N-methylindole which is converted to EPQ through the formation of 5,6-diquinone-N-methylindole at 0.24 V. Thus, thecomplete electrochemical behavior of EP could be detected reliably at the gamma irradiated (50 kGy) SDS-WO_3/GCE when compared to those of other modified electrodes.

Fig. **3B** shows the CVs of 10 µM XAin 0.1 M PBS (pH 7) on bare and modified GCEs with the scan rate of 50 mVs^{-1}. The graph displays that the electro-oxidation of XA using the bare and modified electrodes were asymmetric, indicative of an irreversible process, showing that the anodic peaks in the forward scan have no corresponding discernible reduction peaks on the reverse scan.Thus the electrochemical oxidation of XA proceeds by $2e^-$, $2H^+$ oxidation to form UA at 0.72 V [7]. Clearly, there was a significant increase in the anodic peak current response (5-fold) and lower overpotential(120 mV) were observed for 50 kGy SDS-WO_3/GCE compared to that of bare, pristine and other GI SDS-WO_3/GCEs. The gamma irradiation with a particular dosage of 50 kGy seems to enhance the electroactive surface area and electrical conductivity of SDS-WO_3, which allows two analyte molecules to be oxidized effectively.Therefore, this

proposed electrode (50 kGy GI SDS-WO_3) is more appropriate for the simultaneous detection of EP and XA.

< Preferred position of Fig. 3>

<H2>3.4 Effect of scan rate

The kinetics of the electrode reactions were investigated by studying the effects of scan rate on the peak currents of EP. **Fig. 4A**shows CVs of 10 µM EP on 50 kGy SDS-WO_3/GCE at various scan rates (10 – 500mVs^{-1}). The oxidation peak currents increased with the increase in scan rate. The plot of square of scan rate ($\upsilon^{1/2}$) vs. redox peak currents was linearly associated with corresponding coefficients of 0.9993 and 0.9996 conforming to oxidation and reduction respectively with the linear regression equations of

I_{pa} (µA) = - 3.212 - 71.353 $\upsilon^{1/2}(mVs^{-1})^{1/2}$

I_{pc} (µA) = 0.615 + 49.913 $\upsilon^{1/2}(mVs^{-1})^{1/2}$

This designates that the electrocatalytic reaction of EP at the modified electrode was a diffusion controlled process. The diffusion coefficient (D) and electroactive area (A) have been estimated using Randles–Sevcik equation which relates the peak current for an electron-transfer-controlled process with the square root of the scan rate:

$$i_p = 2.69 * 10^5 n^{3/2} A D^{1/2} C \upsilon^{1/2} \quad (1)$$

where n represents number of electrons transferred and C is the concentration of the species.The diffusion coefficient value (7.13 $*10^{-5}cm^2s^{-1}$) was obtained from the slope of $\upsilon^{1/2}$ vs. I_{pa}. The electroactive surface area values calculated from the above equation illustrates that the 50 kGyGI SDS-WO_3/GCE exhibits higher value (0.061 cm^2) compared to pristine (0.026 cm^2), 100 kGy (0.038 cm^2) and 150 kGy (0.031 cm^2) irradiated SDS-WO_3 electrode surfaces. **Fig. 4B**shows the variation of the peak potentials as a function of the scan rate in order to verify the electrochemical mechanism. From the intercept of υ vs.E_{pa} plot, the formal potential (E^0) of EP was deduced. From the plot (E_{pa} - E^0) vs.lnI_{pa} (**Fig. 4C**), it waspossible to calculate the energy transfer coefficient (α) value and is found to be as 0.47.The number of electrons (n) involved during the oxidation of EP can be calculated from the slope (m) of lnυ vs. E_{pa} (**Fig. 4D**) and substituted in the equation n = [RT/(1-α)mF] and established to be 1.92 (~2). This result was proven by experimentation method and verified to be two electron processes. Further, the heterogeneous rate constant (k^o) value was calculated using Nicholson equation [26] reported for reversible system.

$$\Delta E = k^0 \left(\frac{RT}{\alpha nFD\square} \right)^{1/2} \quad (2)$$

where ΔE represents potential difference,α is the electron transfer coefficient, and F is the Faraday constant.The estimated k^o values for the redox reaction of EP at 50 kGyGI SDS-WO_3/GCE is 21.7 s^{-1}. The higher k^o value for EP at 50 kGyGI SDS-WO_3/GCE clearly indicates

that the redox reaction of EP was superior when compared to the other modified electrodes which promotes the better electrocatalytic oxidation of EP.

Fig. **5A** shows the CVs of 10 µM XA on 50 kGy gamma irradiated SDS-WO_3/GCE at various scan rates (10 – 500 mVs^{-1}) in 0.1 M PBS (pH 7). The anodic peak current increases with the increasing the scan rates and good linearity was established between I_{pa} and $\upsilon^{1/2}$according to the linear equation I_{pa} (µA) = 9.531 – 83.55 $\upsilon^{1/2}(mVs^{-1})^{1/2}$. The system features corresponding to an adsorption controlled process.E^0 was calculated from the intercept of υ vs. E_{pa} plot (**Fig. 5B**).As shown in **Fig. 5C**, the plot (E_{pa}–E^0) vs. lnI_{pa}, α valuewas found to be as 0.36. Based on Laviron's theory, from the slope of E_{pa} against ln ν (**Fig. 5D**), the number of electrons involved during XA oxidation calculated fromRT/αmF and estimated to be 1.85 (~2) and confirmed as two electron process. The standard heterogeneous rate constant (k^0) for the reaction was calculated using the following Laviron equation for an irreversible electrode process [27]:

$$E_{pa} = E^0 + \left(\frac{2.303RT}{\alpha nF}\right) log\left(\frac{RTk^0}{\alpha nF}\right) + \left(\frac{2.303RT}{\alpha nF}\right) log \quad (3)$$

The symbols have their usual meanings. The obtained k^o value for XA at 50 kGy SDS-WO_3/GCE was estimated to be 10.5 s^{-1} which clearly showed that the electrocatlyticof XA was faster than other modified GCE.

< Preferred position of Fig. 4>

< Preferred position of Fig. 5>

<H2>3.5 Effect of pH

Cyclic voltammograms were recorded to study the influence of pH on the electrocatalytic behaviour of EP (10 µM) and XA (10 µM)at 50 kGySDS-WO_3/GCE in 0.1 M PBS (pH 3.0 – 10.0). From **Fig. 6A**, it can be seen that the oxidation peak potential (E_{pa}) of EP and XAdecreases as pH increases demonstrating an intrusion of the protons in the oxidation of both EP and XA. Linear relationship of E_{pa} of EP and XA as function of pH with slopes of 62 and 55 mV/pH respectively were observed, indicating the electron transfer is preceded by a protonation process with the same number of protons involved in the overall electrochemical reaction mechanism. **Fig. 6B** shows the effect of pH on the oxidation peak currents (I_{pa}) of EP and XA at the 50 kGy SDS-WO_3/GCE investigated over the pH range from 3.0 to 10.0. The I_{pa} values of both EP and XA increased with the increase in pH values and reached the maximum at pH 7.0.

With the further increase in pH (> 7.0), the I_{pa} values decreased. At lower pH values (< 7.0), the concentration of H^+ ions in the buffer is higher which suppresses the oxidation process resulting in poor current responses. Similarly, the presence of excessive OH^- ions at higher pH (> 7.0) values diminishes the oxidation process. On the other hand, at neutral pH (7.0), oxidation of both EP and XA was much higher due to unhindered electrocatalytic processes. As a result, the oxidation peak currents of EP and XA were found to higher at pH 7.0. Thus, SDS-WO_3 NPs irradiated with gamma rays at lower dosage (50 kGy) effectively catalyzes both the EP and XA as shown in **Scheme 1**. The gamma induced defects in the facets as seen in FE-SEM pictures (inset of Fig. 2b) and oxygen deficiency caused by localized heating might act as trapping centers leading to the improved electrocatalytic ability of gamma irradiated SDS-WO_3 NPs.

< Preferred position of Fig. 6>

< Preferred position of Scheme 1>

<H2>3.6 Sensitivity and selectivity studies on the simultaneous determination

The simultaneous determination of EP and XA at the 50 kGyGI SDS-WO_3/GCE, was carried out by DPV in the potential range of 0 to 1 V in 0.1 M PBS (pH 7). As shown in **Fig.7A**, the electrochemical response of EP and XA increases linearly with the increase of theirconcentration over the wide range of 0.009 -1000 µM (**Fig. 7B** and **C**). The lowest detection limits were deduced as 1.8 nM and 2.2 nM(S/N=3)for EP and XA respectively.At low concentration range, the response current was due to theadsorptiontransport of EP and XA, whereas at high concentration, the active sites were too fully occupied to further facilitate the transport of both the analyte substrates. Therefore, the corresponding response signal was only due to the diffusion transport according to Fick's law [28] and the linear regression equations are tabulated in Table 1.Though there are large number of reports in the literature dealing with the individual determination of EP and XA, simultaneous detection of EP and XA were not accomplished so far. We have achieved for the first time, the simultaneous detection of EP and XA with the lowest detection limits of 1.8 and 2.2 nM respectively over a very wide linear range of 9 nM to 1 mM for both the analytes. These results confirm the excellent catalytic activity of gamma irradiated SDS-WO_3 towards the detection of EP and XA with high sensitivity and selectivity. In order to make a comparison with recently reported sensors [7, 10, 29-36], the characteristics of different electrochemical sensors for EP and XA detection are summarized in Table 2. It can be seen that the fabricated sensor offered simultaneous detection of EP and XA over very wide linear ranges when compared to that of most sensors reported for detection of either EP or XA individually. It was also noted that there is no report in the literature dealing with the simultaneous detection of EP and XA.

Under the optimum experimental conditions, the influence of various interfering compounds had been investigated on the simultaneous determination of EP and XA.**Fig. 7D** shows the DPVs for the increment of 0.5 µM EP and 0.5 µM XA in the presence of 500 fold excess of ascorbic acid, uric acid, folic acid, guanine, cysteine, ADP, ATP, glucose and 50-fold excess of dopamine, tyrosine, serotonin andnorepinephrine in 0.1 M PBS (pH 7).No significant changes were observed in the peak potentials and response current in the presence of the interfering mixtures (signal change < 2%).No interference was observed for 500-fold excess of metal ions such as Fe^{2+}, Ca^{2+}, Mg^{2+} and Na^+ at 50 kGy gamma irradiated SDS-WO_3 modified GCE by DPV method (Fig. S2).This result indicates that the proposed electrode proved to be a highly selective sensor

for recognition of EP and XA in aqueous solutions. Thus, 50 kGy irradiated SDS-WO_3 NPs is a potential sensing element for construction of sensitive and selective electrochemical sensorsfor real sample analysis.

< Preferred position of Fig. 7>

< Preferred position of Table 1>

< Preferred position of Table 2>

<H2>3.7 Stability and reproducibility

The stability of the modified electrode was examined over a period of a month by storing it in 0.1 M PBS (pH 7) at 4°C for every 2 days intervals. No significant changes were observed during first two weeks and the response yielded over 97.8% of its initial value. Consequently, a small decrease of the peak response current of EP and XA were observed with the relative standard deviation (RSD) of 3.2%, which could be ascribed to the excellent stability of the 50 kGy GI SDS-WO_3 electrode. The reproducibility of the modified electrode was investigated by a series of ten repetitive measurements towards the oxidation of EP and XA mixture.Their response peak current gave reproducible results with the RSD of 3.9%, indicating the excellent reproducibility of the fabricated electrode.

<H2>3.8 Determination of EP and XA in real samples

The reliability and analytical utility of the proposed electrode was tested by the simultaneous determination of EP and XA in human serum samples.The real samples were diluted 10-fold with pH 7.0 phosphate buffer solution and the two biomolecules were determined simultaneously by DPV method.The concentrations of EP and XA were determined using the standard addition technique and the results are summarized in Table 2.In addition to testify the accuracy of this method, the known concentration of EP and XA solution were spiked in the samples and the DPV response signals were measured andreplicated. For the recovery, all the serum samples were diluted 10 times with PBS (pH 7.0). It can be seen that all the spike recoveries values were precise, which revealed that the fabricated sensor can be effectively utilized for the simultaneous determination of EP and XA in real samples.

< Preferred position of Table 3>

<H1>4. Conclusions

In this paper, we demonstrated the application of gamma irradiation for inducing significant changes on the morphological and optical properties of WO_3 NPs. Among various dose levels investigated, 50 kGyirradiated SDS-WO_3 NPs modified GCE acts as an efficient electrocatalystfor the simultaneous determination of EP and XA in the presence of several potentially interfering substances in 0.1 M PBS (pH 7) by voltammetric method. These biomolecules were effectively catalyzed at less positive potentials yielding higher peak current.

The kinetic parameters such as number of electrons transferred, electron transfer coefficient, diffusion coefficient, heterogeneous electron transfer rate constant and pH dependence were investigated. DPV studies exhibits the excellent sensitivity and selectivity towards the simultaneous determination of EP and XA in the presence of 500-fold excess of the interfering agents. The lowest detection limits of 1.8 nM and 2.2 nM(S/N =3)were achieved respectively for EP and XA with dynamic linear range of 9 nM-1 mM for both the molecules.The practical applicability of the fabricated electrode was successfully validated by measuring the concentration of EP and XA in human serum samples.

Acknowledgments

This research was supported by the Inter University Accelerator Centre (IUAC) sponsored project, New Delhi (IUAC-UFR-50312).The authors thank Prof. P. Manisankar and Dr. G. Ravi, Alagappa University for providing FE-SEM and PowderXRD facility.

<REF>References

<BIBL>

[1] E. Wierzbicka, M.S. Mlynska, B. Buszewski, G.D. Sulka,;1; Epinephrine sensing at nanostructured Au electrode and determination its oxidative metabolism, Sens. Actuators B Chem. 237 (2016) 206.

[2] I. Khurana,;1; Essentials of medical physiology, Elsevier publications (2009) <C>ISBN: 978-81-312-1566-1.</C>

[3] T. Vedung, M. Werner, B.O. Ljung, L. Jorfeldt, J. Henriksson,;1; Blood flow to the extensor carpi radialisbrevis muscle following adrenaline infusion in patients with lateral epicondylitis, J. Hand Surg. 36 (2011) 1974.

[4] T.C. Canevari, M. Nakamura, F.H. Cincotto, F.M. de Melo, H.E. Toma,;1; High performance electrochemical sensors for dopamine and epinephrine using nanocrystalline carbon quantum dots obtained under controlled chronoamperometric conditions, Electrochim. Acta 209 (2016) 464.

[5] R.N. Goyal, A.R.S. Rana, Md. A. Aziz, M. Oyama,;1; Effect of gold nanoparticle attached multi-walled carbon nanotube-layered indium tin oxide in monitoring the effect of paracetamol on the release of epinephrine, Anal. Chim. Acta 693 (2011) 35.

[6] T. Tavana, M.A. Khalilzadeh, H. Karimi-Maleh, A.A. Ensafi, H. Beitollahi, D.;1; Zareyee, Sensitive voltammetric determination of epinephrine in the presence of acetaminophen at a novel ionic liquid modified carbon nanotubes paste electrode, J. Mol. Liq. 168 (2012) 69.

[7] R. Ojani, A. Alinezhad, Z. Abedi,;1; A highly sensitive electrochemical sensor for simultaneous detection of uric acid, xanthine and hypoxanthine based on poly(l-methionine) modified glassy carbon electrode, Sens. Actuators B Chem. 188 (2013) 621.

[8] X. Tang, Y. Liu, H. Hou, T. You,;1; A nonenzymatic sensor for xanthine based on electrospuncarbon nanofibers modified electrode, Talanta 83 (2011) 1410.

[9] M. Cui, J. Zhou, Y. Zhao, Q. Song,;1; Facile synthesis of iridium nanoparticles with superior peroxidase like activity for colorimetric determination of H_2O_2 and xanthine, Sens. Actuators B Chem. 243 (2017) 203.

[10] P. Kalimuthu, S.A. John,;1; Simultaneous determination of epinephrine, uric acid and xanthine in the presence of ascorbic acid using an ultrathin polymer film of 5-amino-1,3,4-thiadiazole-2-thiol modified electrode, Anal. Chim.Acta 647 (2009) 97.

[11] P. Kalimuthu, S. Leimkuhler, P.V. Bernhardt,;1; Catalytic electrochemistry of xanthine dehydrogenase, J. Phys. Chem. B 116 (2012) 11600.
[12] S. Mu, Q. Shi,;1; Xanthine biosensor based on the direct oxidation of xanthine at an electrogenerated oligomer film, Biosens. Bioelectron.47 (2013) 429.
[13] H. Zheng, J. Z. Ou, S. M. Strano, B. R. Kaner, A. Mitchell, K. Kalantar-zadeh,;1; Nanostructured tungsten oxide–properties, synthesis, and applications, Adv. Funct. Mater. 21 (2011) 2175.
[14] A.C. Anithaa, N. Lavanya, K. Asokan, C. Sekar,;1; WO_3 nanoparticles based direct electrochemical dopamine sensor in the presence of ascorbic acid, Electrochim. Acta 167 (2015) 294.
[15] V. Hariharan, M. Parthibavarman and C. Sekar,;1; Synthesis of tungsten oxide ($W_{18}O_{49}$) nanosheets utilizing EDTA salt by microwave irradiation method, J. Alloys and Compounds 509 (2011) 4788.
[16] V. Hariharan, S. Radhakrishnan, M. Parthibavarman, R. Dhilipkumar and C. Sekar,;1; Synthesis of polyethylene glycol assisted tungsten oxide nanoparticles for L-dopa bio-sensing applications, Talanta 85 (2011) 2166.
[17] O. Nimittrakoolchai, S. Supothina,;1;High-yield precipitation synthesis of tungsten oxide platelet particle and its ethylene gas-sensing characteristic, Mater. Chem. Phys. 112 (2008) 270.
[18] L.M. Bertus, C. Faure, A. Danine, C. Labrugere, G. Campet, A. Rougier, A. Duta,;1;Synthesis and characterization of WO_3 thin films by surfactant assisted spray pyrolysis for electrochromic applications, Materials Chemistry and Physics 140 (2013) 49.
[19] Q. Huo, D.I. Margolese, U. Ciesla, D.G. Demuth, P. Feng, T.E. Gier, P. Sieger, A. Firousi, B.F. Chmelka, F. Schuth, G.D. Stucky,;1; Organization of Organic Molecules With Inorganic Molecular Species Into NanocompositeBiphase Arrays, Chem. Mater. 6 (1994) 1176.
[20] H. Y. Wang, C. G. Fan,;1; Copper oxide nanostructures: controlled synthesis and their catalytic performance, Solid-State Sci. 16 (2013) 130.
[21] S. Wang, C. An, J. Yuan,;1; Synthetic fabrication of nanoscale MoS_2-based transition metal sulfides, Materials 3 (2010) 401.
[22] M. McPherson, B.K. Jones, T. Sloan,;1; Effects of radiation damage in silicon p-i-n photodiodes, Semicond. Sci. Technol. 12 (1997) 1187.
[23] A.C. Anithaa, K. Asokan, C. Sekar,;1; Highly sensitive and selective serotonin sensor based on gamma ray irradiated tungsten trioxide nanoparticles, Sens. Actuators B Chem. 238 (2017) 667.
[24] J.K. Kim, K. Shin, S.M. Cho, T. Lee, J.H. Park,;1; Synthesis of transparent mesoporous tungsten trioxide films with enhanced photoelectrochemical response: application to unassisted solar water splitting, Energy Environ. Sci. 4 (2011) 1465.
[25] P.V. Narayana, T.M. Reddy, P. Gopal, M.M. Reddy, G.R. Naidu,;1; Electrocatalytic boost up of epinephrine and its simultaneous resolution in the presence of serotonin and folic acid at poly(serine)/multi-walled carbon nanotubes composite modified electrode: A voltammetric study, Mater. Sci. Eng. C 56 (2015) 57.
[26] R.S. Nicholson, I. Shain,;1; Theory of stationary electrode polarography single scan and cyclic methods applied to reversible, irreversible and kinetic systems, Anal. Chem. 36 (1964) 706.
[27] E. Laviron,;1; General expression of the linear potential sweep voltammogram in the case of diffusionless electrochemical systems, Journal of Electroanalytical Chemistry and Interfacial Electrochemistry 101 (1979) 19.

[28] R.B. Bird, W.E. Stewart, E.N. Lightfoot,;1; Transport Phenomena, 2nd ed., Wiley, New York, 2002, 585.
[29] H. Beitollahi, H. Karimi-Maleh, H. Khabazzadeh,;1; Nanomolar and selective determination of epinephrine in the presence of norepinephrine using carbon paste electrode modified with carbon nanotubes and novel 2-(4-Oxo-3-phenyl-3,4-dihydroquinazolinyl)-*N′*-phenyl hydrazinecarbothioamide, Anal. Chem. 80 (2008) 9848.
[30] H. M. Moghaddam, H. Beitollahi, S. Tajik, H. Soltani,;1; Fabrication of a nanostructure based electrochemical sensor for voltammetric determination of epinephrine, uric Acid and folic Acid, Electroanalysis 27 (2015) 2620.
[31] N.Lavanya, E.Fazio, F. Neri, A.Bonavita, S.G. Leonardi, G. Neri, C. Sekar,;1; Simultaneous electrochemical determination of epinephrine and uric acid in the presence of ascorbic acid using SnO2/graphene nanocomposite modified glassy carbon electrode, Sens. Actuators B Chem. 221 (2015) 1412.
[32] E. Akyilmaz, M. Turemis, I. Yasa,;1; Voltammetric determination of epinephrine by White rot fungi (*Phanerochaetechrysosporium* ME446) cells based microbial biosensor, Biosens. Bioelectron.26 (2011) 2590.
[33] H. Ibrahim, Y. Temerk,;1; A novel electrochemical sensor based on B doped CeO_2nanocubes modified glassy carbon microspheres paste electrode for individual and simultaneous determination of xanthine and hypoxanthine, Sens. Actuators B Chem. 232 (2016) 125.
[34] P. Kalimuthu, S. A. John,;1; Simultaneous determination of ascorbic acid, dopamine, uric acid and xanthine using a nanostructured polymer film modified electrode, Talanta 80 (2010) 1686.
[35] B. Dalkiran, C. Kaçar, P.E. Erden, E. Kiliç,;1; Amperometric xanthine biosensors based on chitosan-Co_3O_4-mutiwall carbon nanotube modified glassy carbon electrode, Sens. Actuators B Chem.200 (2014) 83.
[36] N. Lavanya, C. Sekar, R. Murugan, G. Ravi,;1; An ultrasensitive electrochemical sensor for simultaneous determination of xanthine, hypoxanthine and uric acid based on Co doped CeO_2 nanoparticles, Mater. Sci. Eng. C Mater. Biol. Appl. 65 (2016) 278.

</BIBL>
<Figure>Fig. 1. **Powder XRD patterns (A) and UV-visible spectra (B) of SDS-WO_3 (curve a), 50 kGy (curve b), 100 kGy (curve c), and 150 kGy gamma irradiated SDS-WO_3 NPs (curve d). Inset of Fig. 1B shows the plot of samples vs. energy bandgap.**
<Figure>Fig. 2. **FESEM images of (a) non-irradiated SDS-WO_3, (b) 50 kGy, (c) 100 kGy and (d) 150 kGy gamma irradiated SDS-WO_3 NPs; Inset shows the corresponding higher magnification.**

*<Figure>Fig. **3.** Cyclic voltammetry recorded for the 10 μM EP (A) and 10 μM XA (B) at the bare GCE (curve a), pristine SDS-WO_3/GCE (curve b), 50 kGy SDS-WO_3/GCE (curve c), 100 kGy SDS-WO_3/GCE (curve d) and 150 kGy SDS-WO_3/GCE (curve e) at a scan rate of 50 mV s^{-1} in 0.1 M PBS (pH 7.0). Inset of Fig.3A shows the CVs recorded for 10 μM EP at 50 kGy SDS-WO_3/GCE at first cycle (c1), second cycle (c2) and third cycle (c3).*

<Figure>Fig. ***4.*** *(A) Cyclic voltammetry recorded for the 10 μM EP at 50 kGy gamma irradiated SDS-WO_3/GCE in 0.1 M PBS (pH 7.0) at the different scan rates (0.01-0.5 Vs^{-1}). Inset shows the calibration plots for the redox peak currents (I_{pa}) vs. the square root of scan rate ($v^{1/2}$); (B) relationship between the peak potential (E_{pa}) and scan rate (v); (C) experimental variation of peak current (ln I_{pa}) as a function of the difference of $E_{pa} – E^0$; (D) experimental variation of scan rate (ln v) vs. peak potential (E_{pa})*

<Figure>Fig. ***5.*** *Cyclic voltammetry recorded for the 10 μM XA at 50 kGy SDS-WO_3/GCE in 0.1 M PBS (pH 7.0) at the different scan rates (0.01-0.5 Vs^{-1}). Inset shows the calibration plots for the redox peak currents (I_{pa}) vs. the square root of scan rate ($v^{1/2}$); (B) relationship between the peak potential (E_{pa}) and scan rate (v); (C) experimental variation of peak current (ln I_{pa}) as a function of the difference of $E_{pa} – E^0$; (D) experimental variation of scan rate (ln v) vs. peak potential (E_{pa}).*

<Figure>Fig. ***6.*** *(A) Plot of oxidation peak potential of 10 μM EP and XA vs. pH (3.0 – 10.0); (B) The corresponding oxidation peak current vs. pH (3.0 – 10.0) in PBS at a scan rate of 50 mVs^{-1} for 50 kGy SDS WO_3/GCE.*

<Figure>Fig. **7.** (A) Differential pulse voltammograms of 50 kGy SDS-WO_3/GCE in 0.1 M PBS (pH 7.0) containing different concentrations of EP and XA (0.009-1000 μM); (B) and (C) show the plots of the electrocatalytic oxidation peak current as a function of EP and XA concentration respectively; (D) Selective response of 50 kGy SDS-WO_3/GCE for the increment of 0.5 μM EP and 0.5 μM XA with successive additions of interferents in the sequence of (a) ascorbic acid, (b) dopamine, (c) tyrosine, (d) serotonin, (e) norepinephrine, (f) uric acid, (g) folic acid, (h) guanine, (i) cysteine, (j) ADP, (k) ATP and (l) glucose in 0.1 M PBS (pH 7.0).

<Figure>**Scheme 1** Electrocatalytic oxidation of epinephrine and xanthine at 50 kGy SDS-WO_3 NPs.

<Table>Table 1 Analytical characteristics for simultaneous determination of EP and XA at the 50 kGy SDS-WO_3 modified GC electrode.

Analyte	Linear Range (μM)	Linear regression equation (I_{pa}: μA, C: μM)	Correlation coefficient	Detection limit (nM)	RSD %
EP	0.009-100	$I_{pa} = 1.011\ C_{EP} - 0.663$	0.9995	0.7	1.7
	100-1000	$I_{pa} = 0.061.011\ C_{EP} - 112.895$	0.9996	3.0	1.4
XA	0.009-100	$I_{pa} = 0.797\ C_{XA} - 0.518$	0.9992	0.4	1.6
	100-1000	$I_{pa} = 0.054\ C_{XA} - 88.294$	0.9994	4.0	1.5

<Table>Table 2 Comparison of the fabricated sensor with the EP and XA sensors recently reported in the literature

Electrode	EP (μM)		XA (μM)		Ref.
	LR	LOD	LR	LOD	
p-ATT/GCE	0.04-40	270 x 10^{-6}	-	-	[10]
2PHCM/CNPE	0.05-550	0.0096	-	-	[29]
2,7-BFGPE	0.05-550	0.027	-	-	[30]
SnO_2/graphene/GCE	0.5-200	0.017	-	-	[31]
Gelatine- glutaraldhyde P. chyrsosporium/Pt	5-100	1.04	-	-	[32]
CeO_2 NCs /GCPE	-	-	0.198-9.45	0.0036	[33]
Poly(ATD)/GCE	-	-	5-45	0.59	[34]
Co_3O_4/MWCNT/CS/GCE	-	-	0.2-16	0.2	[35]
Poly(L-methionine)/GCE	-	-	0.02-0.1	0.004	[7]
Co doped CeO_2 NPs/GCE	-	-	0.1-1000	0.096	[36]
50 kGy GI SDS-WO_3 / GCE	**0.009-1000**	**0.0018**	**0.009-1000**	**0.0022**	**This work**

2PHCM/CNPE: 2-(4-oxo-3-phenyl-3,4-dihydro-quinazolinyl)-*N*′-phenyl-hydrazinecarbothio-amide modified carbon nanotube paste electrode
p-ATT: Poly (5-amino-1,3,4-thiadiazole-2-thiol)
2,7-BFGPE: 2,7-bis(ferrocenyl ethyl) fluoren-9-one and graphene nanosheets

<Table>Table 3 Simultaneous determination of EP and XA in human serum samples.

No. of Exp	EP spiking (nM)	XA spiking (nM)	EP Found (nM)	XA Found (nM)	Recovery (%)		RSD (%)	
					EP	XA	EP	XA
1	10	10	9.93	10.09	99.7	102.5	3.1	2.4
2	25	25	25.15	25.93	98.5	103.6	1.9	2.7
3	50	50	50.87	50.13	102.4	99.5	2.5	3.3

TDENDOFDOCTD